

Integrated Rudder/fin Concise Control based on Frequency Domain Analysis

W Guan*, ZJ Su, GQ Zhang

Navigation Department, Dalian Maritime University (DMU)

Linghai Road NO.1, 116026, Dalian City, Liaoning Province, China, telp: +86-18900982591

Corresponding author, e-mail: gwwtxdy@163.com, suzuojing@163.com, zgq_dlm@163.com

Abstract

This paper describes a concise robust controller design of integrated rudder and fin control system in use of the closed loop gain shaping algorithm (CGSA) strategy. Compared with the arbitrary selection of weighting function in integrated rudder and fin H_{∞} mixed sensitivity control design procedures, the CGSA methods provided a relatively more straightforward and concise design method. Simulations were described that the overall performance of each CGSA rudder and fin control loop and the interaction between them. Hence, it can be concluded that the integrated rudder and fin CGSA control scheme is very suitable to present and indeed feasible for future practical application.

Keywords: *integrated rudder/fin, frequency domain analysis, concise robust control, CGSA*

Copyright © 2013 Universitas Ahmad Dahlan. All rights reserved.

1. Introduction

As we know, the ship sailing in seaways usually endures large roll and yaw motions due to waves, which may lead to seasickness, disturbance of ship operations and stability loss, etc. Especially roll motion may be the most undesirable phenomena for crews since it may cause some inconvenience and accidents at sea. Therefore several techniques, either active or passive, for avoiding large rolling motions have been employed. To date, fin stabilizer has been recognized as the most propitious device which delivers an unparalleled degree of roll stabilization. Furthermore it has been observed that when the rudder 'put-over' the ship, the ship initially heels inwards before attaining the steady state, and this initial roll angle usually occurs before the ship enters into any yaw motion. Suggesting that the characteristic ephemeral rudder induced roll may be used congress with fin to enhance roll stabilization without significant interference to the heading angles. The potential of rudder roll stabilizer (RRS) had been recognized and some studies conducted to assess its feasibility [1]. Especially the use of the existing slow rudder to assist the stabilizing fins appears to provide an inexpensive method for improving the roll reduction currently, without the requirement to provide additional systems or enhance those already fitted [2]. This approach has the additional benefit of providing the flexibility to engage stabilization as dictated by operational requirements. However, the design of the constituent controllers of an integrated fin and rudder stabilization system presents a complex control engineering problem since the ship's dynamics are multivariable and uncertainty exists on account of empirically derived hydrodynamic coefficients. Also, the environmental disturbances such as wind, wave cannot be modeled precisely [3]. Therefore, how to select a suitable integrated rudder and fin controller to reduce the ship roll and yaw motion in rough waves is an important technology. The H_{∞} mixed sensitivity robust control approach and μ -synthesis technique had offered a way to solve this problem [4-7]. But the above robust algorithms require careful selection of the weighting function because the weighting functions embody the desired characteristics in terms of performance, also the solving process is complex and the final solution to a great extent depends on the selection of the weighting matrixes which are almost arbitrary [8]. Especially for integrated rudder and fin control system, the controllers are so complex and arbitrary that it cannot be feasible for practical engineering application. Therefore, a robust control strategy named close-loop gain shaping algorithm [9] (CGSA) will be utilized in the rudder and fin integrated controller design on account of its ability to deliver controller which can guarantee levels of robust stability and control performance.

2. System Descriptions

2.1. Multivariable Ship Rudder and Fin Model

Figure 1 shows the integrated rudder and fin control arrangements. Where φ is the roll angle, ψ is the yaw angle, α is the commanded fin angle, δ is the commanded rudder angle. Take $y_1 = \varphi$, $y_2 = \psi$ as the system output and α , δ as the system input, then take the Laplace transform, therefore the transfer function of multivariable rudder and fin integrated system could be obtained and it can be expressed as equation (1),

$$\begin{bmatrix} \varphi \\ \psi \end{bmatrix} = \begin{bmatrix} G_{11}(s) & G_{12}(s) \\ G_{21}(s) & G_{22}(s) \end{bmatrix} \begin{bmatrix} \alpha \\ \delta \end{bmatrix} = \begin{bmatrix} \frac{b_{11}}{s^2 - a_{11}s - a_{12}} & \frac{b_{12}}{s^2 - a_{11}s - a_{12}} \\ \frac{b_{21}}{s^2 - a_{21}s} & \frac{b_{22}}{s^2 - a_{21}s} \end{bmatrix} \begin{bmatrix} \alpha \\ \delta \end{bmatrix} \quad (1)$$

Where the parameters a_{11} , a_{12} , a_{21} , b_{11} , b_{12} , b_{21} , b_{22} can be estimated according to the reference [10] where reader can get the details. In this paper, the motor vessel **YUKUN** is considered to illustrate the application of the proposed concept. Therefore, the parameters of the equation (1) are calculated and given in table 1.

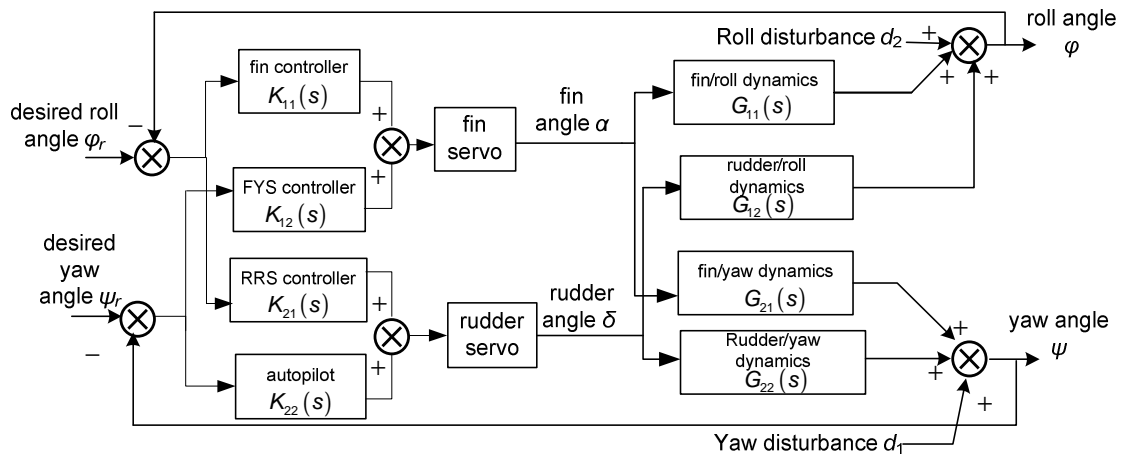


Figure 1. Integrated rudder and fin control arrangements

Table 1. Parameters of multivariable model of the ship **YUKUN**

Parameters	a_{11}	a_{12}	a_{21}	b_{11}	b_{12}	b_{21}	b_{22}
Value	-0.0763	-0.3588	-0.2706	-0.0774	0.0182	-0.0014	0.0166

2.2. Rudder Dynamics

The rudder can be utilized for both course-keeping and roll stabilization in this literature. In its latter role, the rudder employs the peculiar characteristic that when the rudder is ‘put-over’ the ship develops a transitory inward heel which appears to be outward heel before attaining the steady state. Such behaviour is illustrated in Figure 2 which shows the roll and yaw motions with the typical time scales involved.

Furthermore, the open-loop frequency spectra of $G_{22}(s)$ and $G_{12}(s)$ are shown in Figure 3. It can be seen that the use of rudders for roll stabilization will not have a detrimental effect on the ship yaw motion in low frequency region (below 1.0 rad/s) since a frequency separation between the roll and yaw channels will render the cross-coupling negligible. Although Blanke and Christensen suggest that the yaw/roll coupling is significant in high frequency region (above 1.0 rad/s) [11], Amerongen has shown that the appropriate filters can be installed as a contingency against this scenario [1].

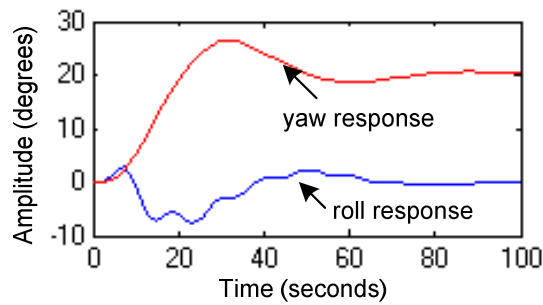


Figure 2. Rudder-induced ship motion

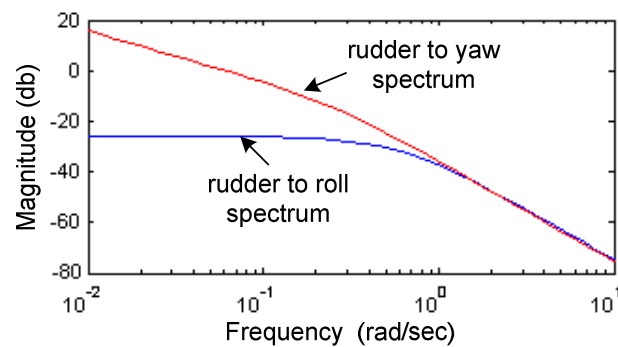


Figure 3. Typical roll and yaw spectrums

2.3. Rudder and Fin Servomechanism

Since the main objective of this project is to utilize the existing rudders to assist the roll reduction, it may be judicious to examine the capabilities of the rudder servomechanisms to perform in their new roles. Their effectiveness of roll stabilization is completely dependent upon the servomechanism which activates the control surfaces. It is illustrated in Figure 4 which shows a typical frequency response of ship roll motion and rudder servomechanism. If the servomechanism frequency response encompasses the entire ship roll response, then it will actively stabilize at all frequencies of motion. Otherwise, the ship roll response beyond the servomechanism response, the sea-induced roll will be amplified. It should also be noted that there are two saturation nonlinearities associated with their mechanics for both the fin and rudder hydraulics, which are shown in Figure 5.

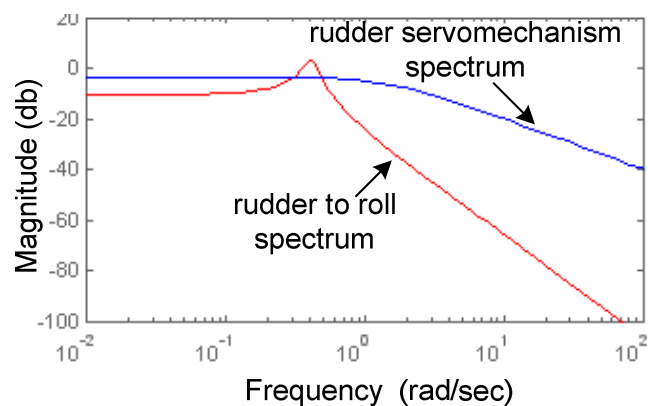


Figure 4. Typical roll response and rudder servomechanism frequency response

The first saturation nonlinearity models the maximum angles of excursion. The second saturation element models the slew rate nonlinearity. For adequate stabilization, the slew of the servomechanism is very important since it is the nonlinearity to the extent that their maximum rate is restricted [12]. In this paper, the maximum angle of excursion is ± 22 degrees for the fins, and ± 28 degrees for rudder. The maximum slew of ± 4.8 degrees per seconds and ± 6 degrees per seconds for fins and rudders slew rate respectively.

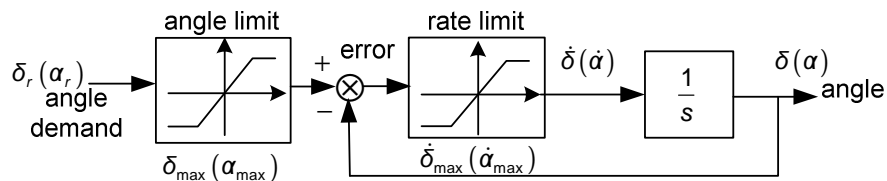


Figure 5. Rudder/fin servomechanism model

3. Control Arrangements

3.1. Closed Loop Gain Shaping Algorithm

The ship operating environment is usually varied due to the wind, waves and the other sea states changes. Also, the mathematical models of the actual ships are inherently uncertain due to hydrodynamic coefficients changes, unmodelled dynamics and time-delays, sensor noise inputs. As a consequence, it is not clear whether the real controlled system will remain stable or the performance will be reasonable, using the controller based on the approximate plant model. The closed-loop gain shaping algorithm (CGSA), which simplified H_∞ mixed sensitivity robust design procedure, may be a good solution to this problem.

The H_∞ mixed sensitivity robust control procedure as defined in Doyle [13], requires careful selection of the weighting function because the weighting functions directly embody the desired characteristics in terms of performance, thus the solving process is complex and the final solutions to a great extent depend on the selection of the weighting matrix which is almost arbitrary. Inspired by loop shaping theory, the CGSA is formed based on the observation on the characteristics of the singular value curves of H_∞ mixed sensitivity functions as well as the correlativity between the sensitivity function $S(s)$ and the complementary sensitivity function $T(s)$ as shown in Figure 6. The essence of the CGSA is to construct $T(s)$ using four parameters with engineering sense (such as bandwidth frequency, high frequency asymptote slope, the largest singular value and the peak value of the closed-loop frequency spectrum) and then the controller $K(s)$ is reversely deduced out without selecting any weighting functions. The shape of $S(s)$ is fixed indirectly because of the relationship between $S(s)$ and $T(s)$ ($T(s) + S(s) = I$). Therefore the CGSA methodology can guarantee fundamentally that the designed control system will be relatively concise as well as fine robust performance and robust stability.

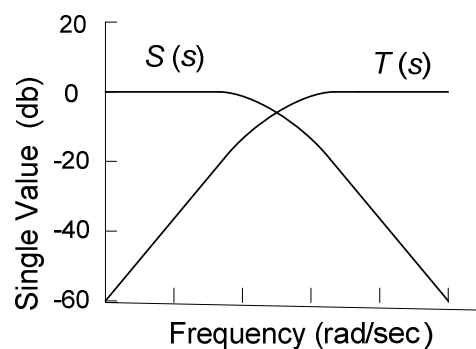


Figure 6. Typical $S(s)$ & $T(s)$ singular value of high frequency asymptote slope

For further discussing CGSA controller design, a schematic closed-loop feedback control system is illustrated in Figure 7. It is assumed that the structure of the uncertainty in the Figure 7 can be represented by multiplicative uncertainty at the plant input. Along with the representation of the nominal plant transfer function G_0 , the multiplicative transfer function Δ is the representation of mathematical uncertainty and it can be represented as

$$G_{\Delta}(s) = G_0(s)(1 + \Delta) \tag{2}$$

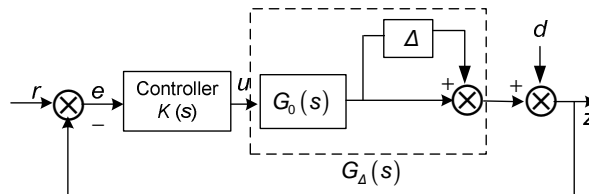


Figure 7. Standard feedback control system with multiplicative uncertainty

Although the transfer function of Δ is unknown, it must be assumed to be stable and bounded by the H_{∞} norm condition given in inequation (3),

$$\|\Delta\|_{\infty} < \gamma \tag{3}$$

where γ is a scalar search variable and its value will be discussed in the next section.

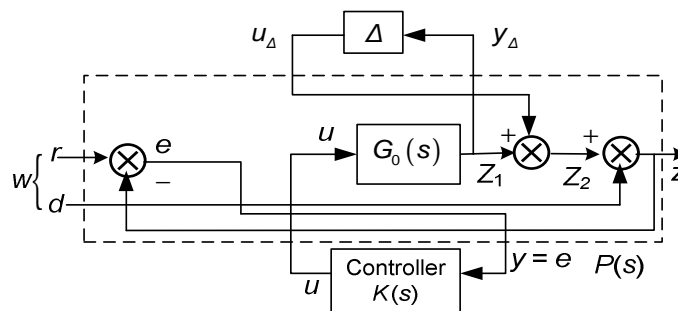


Figure 8. Standard H_{∞} design augmented systems

Referring to the control system shown in Figure 7, where $K(\bullet)$ represents the controller; $d(\bullet)$ is the environmental disturbance; $r(\bullet)$ is the reference signal; $e(\bullet)$ is the error signal; $u(\bullet)$ is the control action and $z(\bullet)$ is the output signal. To proceed with the controller synthesis, the feedback control system depicted in Figure 7 is represented in the standard H_{∞} control configuration as shown in Figure 8. The standard H_{∞} design problem is formulated as follows and given a state space realization of an augmented plant $P(s)$

$$\begin{bmatrix} y_{\Delta} \\ z \\ y \end{bmatrix} = P(s) \begin{bmatrix} u_{\Delta} \\ r \\ d \\ u \end{bmatrix} = \begin{bmatrix} 0 & 0 & 0 & G_0 \\ 1 & 0 & 1 & G_0 \\ -1 & 1 & -1 & -G_0 \end{bmatrix} \begin{bmatrix} u_{\Delta} \\ r \\ d \\ u \end{bmatrix} = \begin{bmatrix} P_{11} & P_{12} \\ P_{21} & P_{22} \end{bmatrix} \begin{bmatrix} u_{\Delta} \\ r \\ d \\ u \end{bmatrix} \tag{4}$$

Taken the augmented plant $P(s)$ and controller $K(s)$ as one augmented plant, along with the lower linear fractional transform, the all controllers that stabilize the closed-loop is

$$N_{\Delta}(s) = P_{11} + P_{12} (I - KP_{22})^{-1} KP_{21} = \begin{bmatrix} N_{11}(s) & N_{12}(s) \\ N_{21}(s) & N_{22}(s) \end{bmatrix} \quad (5)$$

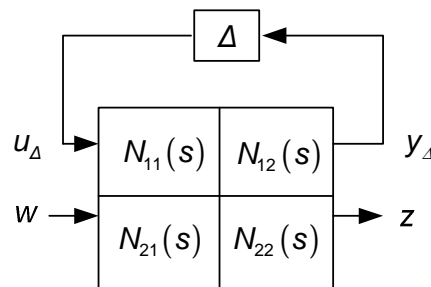


Figure 9. Standard H_{∞} design robust stabilization synthesis system

As shown in Figure 9, the perturbation transfer function between $u_{\Delta}(s)$ and $y_{\Delta}(s)$ is $N_{11}(s)$ and its presentation is

$$N_{11}(s) = \frac{u_{\Delta}(s)}{y_{\Delta}(s)} = \frac{-G_0(s)K(s)}{1+G_0(s)K(s)} \quad (6)$$

Thus it is possible to define the problem as design an H_{∞} robust controller $K(s)$ that will stabilize the close-loop system for all plant uncertainties represented by Δ . Therefore, according to the small gain theory, it is required the equation as defined in equation (6) has its H_{∞} norm less than unity.

$$\|N_{11}(s) \Delta\|_{\infty} \leq \|N_{11}(s)\|_{\infty} \|\Delta\|_{\infty} \leq 1 \quad (7)$$

As we known, the complementary sensitivity function $T(s) = G_0(s)K(s)/(1+G_0(s)K(s))$, hence the equation (7) can be represented as

$$\|G_0(s)K(s)/(1+G_0(s)K(s)) \Delta\|_{\infty} = \|T(s) \Delta\|_{\infty} \leq \|T(s)\|_{\infty} \|\Delta\|_{\infty} \leq 1 \quad (8)$$

Then the in equation (9) can be arranged to show the bounds of the plant uncertainties

$$\|\Delta\|_{\infty} \leq \|T(s)\|_{\infty}^{-1} = \|1+1/G_0(s)K(s)\|_{\infty} \quad (9)$$

Therefore, there exists an admissible stabilizing controller of closed-loop system if the H_{∞} norm of multiplicative uncertainty function Δ meets

$$\|\Delta\|_{\infty} < 1 \quad (10)$$

Furthermore, it should also be noted that: in order to minimize the effects of the multiplicative uncertainties and the disturbances on the controller, the sensitivity and control action of the controller $K(s)$ must be shaped by the appropriate choice of the complementary sensitivity function $T(s)$. However suitable functions are often be obtained after a complex trail, the more concise methods of selecting functions have been given by Grimble [14] and Maciejowski [15]. According to these reference assuring a small sensitivity function $S(s)$ always leads to good disturbance attenuation and a good command following, related to the system bandwidth. From equation (8), it is concluded that a small complementary sensitivity $T(s)$ implies moderate controller gains and good robustness to multiplicative uncertainties. However from the definition of $S(s)$ and $T(s)$, they have relationship $S(s) + T(s) = I$. This identity indicates a fundamental trade-off between performance and robustness, since $S(s)$ and $T(s)$ cannot be

made small simultaneously. To overcome this problem, these functions are made small at different frequencies. Usually, reference signals and disturbances spectra are concentrated at low frequencies, whilst the noise spectrum extends over a wider range. The solution almost universally adopted is to make $S(j\omega)$ small at low frequencies and $T(j\omega)$ small at high frequencies.

As shown in Figure 6, in order to guarantee the robust performance, the frequency spectrum of complementary sensitivity function $T(s)$ is high at low frequencies and roll off at high frequencies; The frequency spectrum of sensitivity function $S(s)$ is fixed indirectly because of the relationship between $S(s)$ and $T(s)$ ($T(s) + S(s) = I$). At the same time, the largest singular value is less than one for achieving a good tracking performance without steady-state error. The suitable selection of system bandwidth and the high frequency spectrum asymptote slope of $T(s)$ can determine the tracking ability and disturbance attenuation characteristics.

In this paper, MIMO closed-loop feedback system is of interest. According to the equation $T(s) = G_0 K / (I + G_0 K)$, we can get the corresponding controller for MIMO system

$$K(s) = G_0(s)^{-1} [I(s) - T(s)]^{-1} T(s) \quad (11)$$

The controller $K(s)$ can be derived from formula (11) for a constructed complementary sensitive function matrix $T(s)$ such as equation (12).

$$T(s) = \begin{bmatrix} \frac{1}{(T_{11}s+1)^2} & 0 \\ 0 & \frac{1}{(T_{22}s+1)^2} \end{bmatrix} \quad (12)$$

where, the diagonal elements of $T(s)$ can be set as second-order inertial components with the largest singular values being 1 such that it guarantees there is no overshoot in the closed-loop feedback control system. While the non-diagonal elements of $T(s)$ are all set as 0 for decoupling the different control channel. T_{11} and T_{22} are tuning parameters of the resulting CGSA controller and they can determine the tracking ability and disturbance attenuation characteristics of the MIMO closed-loop feedback system, so that selection of their values requires a lot of trials data. Therefore, a MIMO CGSA controller was obtained. If a more accurate controller is required, the high frequency spectrum asymptote slope of $T(s)$ can also be assigned to be -60 dB/dec and the diagonal elements of $T(s)$ could be set as the third-order inertial components. But the new CGSA controller will cause a corresponding increase of controller complexities. Thus a trade-off between accuracy and complexity must be made.

3.2. CGSA Controller Design for Ship Integrated Rudder and Fin System

The closed-loop system described in Figure 7 defines the control problem well but it is not immediately apparent how this translates to a practical system that can be used for controller design. Hence a practical system that can be used for controller design structure is shown in Figure 10.

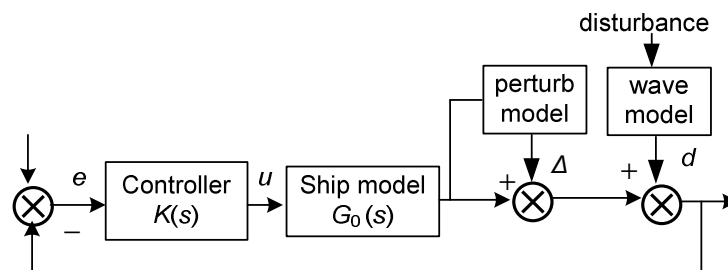


Figure 10. Practical system used in controller design

Where $K(\bullet)$ represents the integrated rudder/fin controller; $G_0(\bullet)$ represents the ship rudder/fin integrated system model; $d(\bullet)$ is the wave disturbance to roll/yaw; $r(\bullet)$ is the reference signal; $e(\bullet)$ is the error signal; $u(\bullet)$ is the control action signal; $\Delta(\bullet)$ represents the uncertainties of ship rudder/fin integrated system; The equation (13) shows the ship rudder and fin integrated controller derived from the equation (1), (11) and (12),

$$K(s) = \begin{bmatrix} K_{11}(s) & K_{12}(s) \\ K_{21}(s) & K_{22}(s) \end{bmatrix} \quad (13)$$

where,

$$K_{11}(s) = \frac{b_{22}(s^2 - a_1s - a_{12})}{T_{11}(b_{11}b_{22} - b_{12}b_{21})(T_{11}s + 2)s}, \quad K_{12}(s) = \frac{-b_{12}/(b_{11}b_{22} - b_{12}b_{21})(s - a_{21})}{T_{22}(T_{22}s + 2)},$$

$$K_{21}(s) = \frac{b_{21}(s^2 - a_1s - a_{12})}{T_{11}(b_{11}b_{22} - b_{12}b_{21})(T_{11}s + 2)s}, \quad K_{22}(s) = \frac{b_{11}/(b_{11}b_{22} - b_{12}b_{21})(s - a_{21})}{T_{22}(T_{22}s + 2)}.$$

4. Simulations and Analysis

In this paper, the motor vessel **YUKUN** is considered to illustrate the application of the following concept in this paper. The parameters of the integrated rudder and fin CGSA controller T_{11} and T_{22} are set as 80 and 4 respectively. The 4th order Runge-Kutta method is applied to solve the following simulation of the ship motion responses. It must be assumed that the decoupled rudder and fin control channel was employed, hence the control signals can be derived separately and form a composite rudder demand or fin demand. Then it, although it is difficult, could control two interactive motions by employing only one variable. In the following section, each control channel will be discussed.

4.1. Rudder Control Loop Analysis

The rudder to roll stabilizer (RRS) $K_{21}(s)$ is to reduce the roll motion with the rudder. The rudder to yaw controller $K_{22}(s)$ is considered to act two modes, namely course-changing and course-keeping and the final controller requires both two modes to operate together. The controller design procedure has been described in the above section, and the frequency response of the $K_{21}(s)$ and $K_{22}(s)$ are illustrated separately in Figure 11.

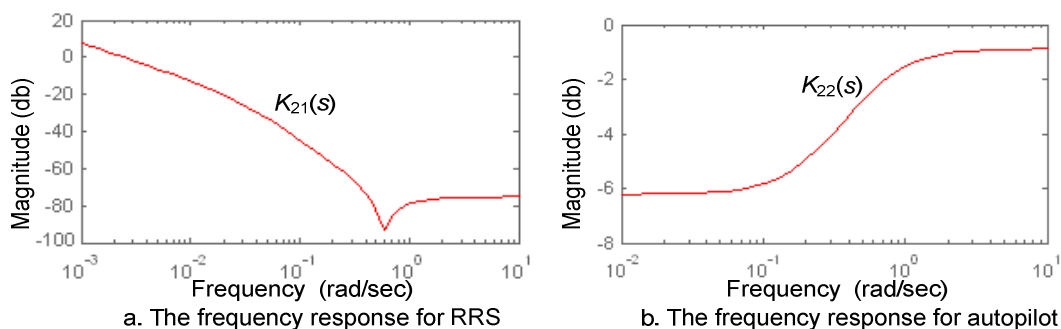


Figure 11. The frequency response for rudder loop

The ship motion around roll resonance is greatest as frequency increases or decreases. Hence the controller $K_{21}(s)$ should be relatively lower where the roll resonance frequency (0.61 rad/sec). Since it is physically difficult to control roll disturbance at high and low frequencies regions, the controller $K_{21}(s)$ rolls off above and below the ship roll resonance frequency. Because of the engineering constraints on the rudder, such as the slew rate, it is required that the upper frequency band (above 0.9 rad/sec) of the controller $K_{21}(s)$ must be restricted to prevent the rudder saturation.

The autopilot controller $K_{22}(s)$ determines the tracking ability and disturbance attenuation characteristics of the ship yaw motion. In general the yaw disturbance are mostly in the low frequency region (below 1.0 rad/sec) and the high frequency rudder activity is not desirable since it may interfere with the fin stabilization system and exacerbate the rudder servomechanisms, hence the controller $K_{22}(s)$ is kept lower in low frequency region. Also, due to the possible interaction between the rudder roll stabilization system and the autopilot especially in the high frequency region as shown in Figure 3, the controller $K_{22}(s)$ should be kept larger than $K_{21}(s)$ in the high frequency region (above 0.1 rad/sec).

Having independently analysis the RRS controller $K_{21}(s)$ and autopilot $K_{22}(s)$, the degree of interaction between the two control loop is investigated. The degree of cross-coupling is established thus: the autopilot response to yaw disturbance with and without RRS is investigated, and then the RRS response to roll disturbance with and without the autopilot is determined.

4.1.1. RRS Repercussion on Autopilot

The transfer function between the yaw angle $\psi(s)$ and yaw disturbance $d_1(s)$ is analyzed.

$$\text{Without RRS} \quad \psi(s)/d_1(s) = 1/(1 + K_{22}(s)G_{22}(s)) \quad (14)$$

$$\text{With RRS} \quad \psi(s)/d_1(s) = 1/(1 + K_{22}(s)G_{22}(s)/K_{21}(s)G_{12}(s)) \quad (15)$$

Figure 12 depicts the yaw disturbance attenuation characteristic obtained by employing the CGSA controller with and without the RRS control signal. It is pertinent to mention that the yaw disturbance lies in low-frequency region (below 1.0 rad/sec), and there is an improvement in the disturbance attenuation performance in the low frequency region with RRS loop. Especially, the difference in the high frequency responses is impressive. The controller with RRS control signal rolls off gently as the increase of the frequency, whereas the controller without RRS increases, which indicates that the controller with RRS has larger tendency to attenuate the high frequency yaw disturbances. Therefore, it can be concluded that the autopilot controller with RRS signal has much better yaw disturbance attenuation performance especially in the frequency response region above 0.01 rad/sec.

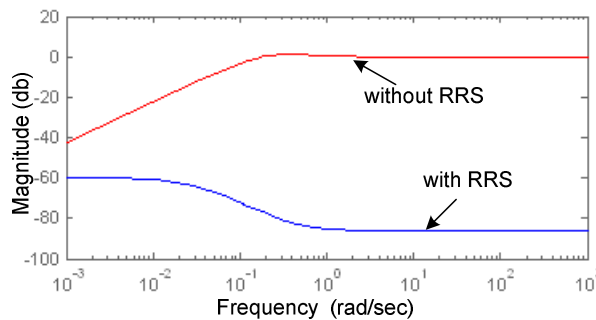


Figure 12. Yaw sensitive function with and without RRS

4.1.2. Autopilot Impact on RRS

The transfer function between the stabilized roll angle $\varphi(s)$ and roll disturbance $d_2(s)$ is also analyzed.

$$\text{Without autopilot} \quad \varphi(s)/d_2(s) = 1/(1 + K_{21}(s)G_{12}(s)) \quad (16)$$

$$\text{With autopilot} \quad \varphi(s)/d_2(s) = 1/(1 + K_{21}(s)G_{12}(s)/K_{22}(s)G_{22}(s)) \quad (17)$$

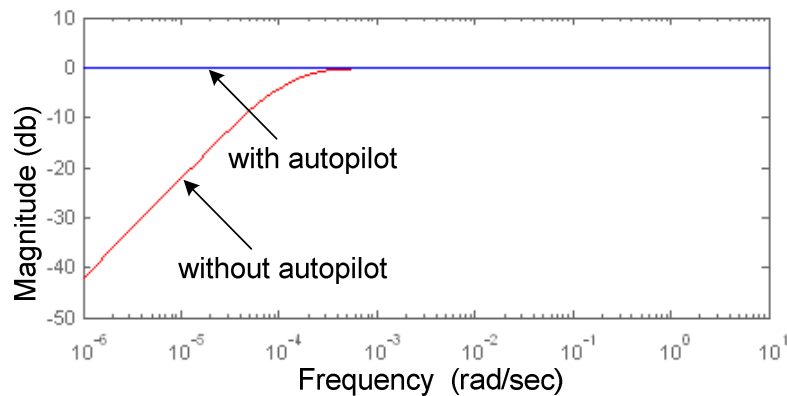


Figure 13. Roll sensitive function with and without autopilot

Figure 13 depicts the roll disturbance attenuation characteristics by employing the CGSA RRS controller with and without the autopilot control signal. We can see that the responses of RRS controllers with the autopilot are identical with RRS controller without autopilot in higher frequency region above 0.001 rad/sec. One of main reasons for this is that the non-diagonal elements of the CGSA constructed $T(s)$ are all set as 0 for decoupling the different control channel. Although in low frequency region (below 0.001 rad/sec) the roll disturbances are attenuated to a greater extent without the autopilot cross-coupling interaction, this low frequency region is out of interest because the roll disturbance mostly lies in the frequency region of 0.1 to 1.0 rad/sec. Therefore, the autopilot control signal has negligible impact on the RRS control loop.

4.2. Fin Control Loop Analysis

In this part, we will discuss the fin control loop. In order to reduce the action of the disturbance waves, the active fin roll stabilizer $K_{11}(s)$ may be the most effective in the roll reduction control system. The fin yaw stabilizer (FYS) $K_{12}(s)$ is also discussed in this section, although the hull design and position of the stabilizing fins resulting in a negligible fin to yaw motion is reported in [16], its effect on heading stability was also explored. The frequency response of the control loop $K_{11}(s)$ and $K_{12}(s)$ are illustrated separately in Figure 14.

Confidence in the ship roll motion around roll resonance point is greatest as frequency increases or decreases. Hence the fin roll stabilizer $K_{11}(s)$ should relatively lower in the ship roll resonance frequency (0.61 rad/sec). And the controller $K_{11}(s)$ rolls off above and below the ship roll resonance frequency since it is physically difficult to control roll disturbance at high and low frequencies regions. Especially for the engineering constraints on the fins, such as the slew rate, it is required that the upper frequency region (above 0.9 rad/sec) of the controller $K_{11}(s)$ must be restricted to prevent the fin servomechanism saturation.

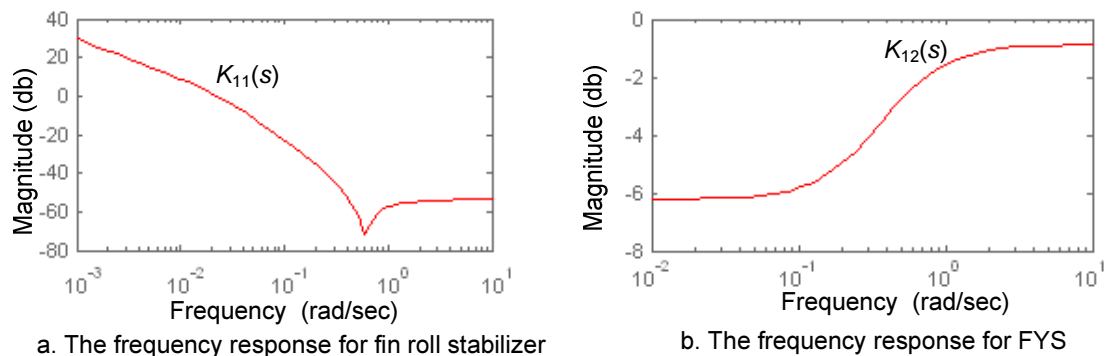


Figure 14. The frequency response for fin control loop

The FYS controller $K_{12}(s)$ is auxiliary stabilizer for the ship course tracking ability and it will eliminate the yaw motion noise which produced by the fins and rudders. In general, the yaw noise disturbances are mostly in the lower frequency region (below 1.0 rad/sec) and the high frequency fin activity is not desirable since it may exacerbate the fin servomechanisms. Also, in order to avoid the possible interaction between the fin roll stabilization system and the FYS system in the high frequency region, the controller $K_{12}(s)$ should be kept larger than $K_{11}(s)$ in the high frequency response region (above 0.1 rad/sec).

Having independently analysis the fin roll stabilizer (FRS) $K_{11}(s)$ and FYS $K_{22}(s)$, the interaction between the two control loops is investigated. The degree of cross-coupling is determined thus: the fin roll stabilization response to roll disturbance with and without fin yaw stabilizer is firstly investigated, and then the FYS response to yaw disturbance with and without the fin roll stabilizer is determined.

4.2.1. FYS Repercussions on FRS

The transfer function between the stabilized roll angle $\varphi(s)$ and roll disturbance $d_2(s)$ is analyzed.

$$\text{Without FYS} \quad \varphi(s)/d_2(s) = 1/(1 + K_{11}(s)G_{11}(s)) \quad (18)$$

$$\text{With FYS} \quad \varphi(s)/d_2(s) = 1/(1 + K_{11}(s)G_{11}(s)/K_{12}(s)G_{21}(s)) \quad (19)$$

Figure 15 depicts the roll disturbance attenuation characteristic obtained by employing the CGSA fin roll stabilizer with and without the FYS control loop. It is shown that as the increase of the frequency, the roll disturbances are amplified evidently for both the cases. Comparing to the control loop with the FYS, the controller without FYS improves the system bandwidth and has larger tendency to response the roll disturbance in the frequency below 0.05 rad/sec. It also should be noticed that the difference in the high frequency response region (above 0.05 rad/sec) demonstrate that the controller without FYS has better roll disturbance attenuation characteristics. Therefore, it can be conclude that the FYS control loop degrades the roll disturbance attenuation performance of FRS.

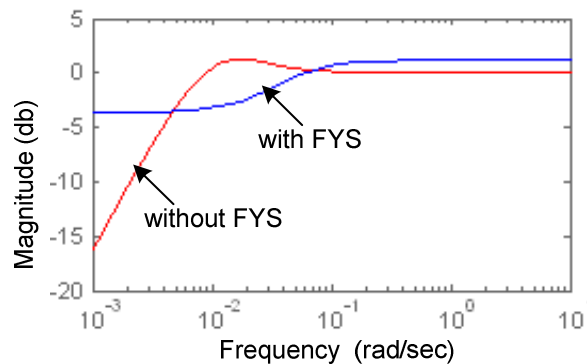


Figure 15. Roll sensitive function with and without fin yaw stabilization

4.2.2. FRS Impact on FYS

The transfer function between the $\psi(s)$ and yaw disturbance $d_1(s)$ is analyzed.

$$\text{Without FRS} \quad \psi(s)/d_1(s) = 1/(1 + K_{12}(s)G_{21}(s)) \quad (20)$$

$$\text{With FRS} \quad \psi(s)/d_1(s) = 1/(1 + K_{12}(s)G_{21}(s)/K_{11}(s)G_{11}(s)) \quad (21)$$

Figure 16 depicts the yaw disturbance characteristics by employing the FYS control loop with and without the FRS. It is noticed that the controller with FRS could improve the

system bandwidth as can be seen from the roll off feature at the frequency region from 0.01 to 1.0 rad/sec where the yaw disturbances are encompassed. That is main reason that, with the FRS coupling efforts, the FYS has larger tendency to attenuate the yaw disturbance attenuation. Therefore it can be concluded that the FYS with FRS has much better yaw disturbance attenuation performance especially in the higher frequency region.

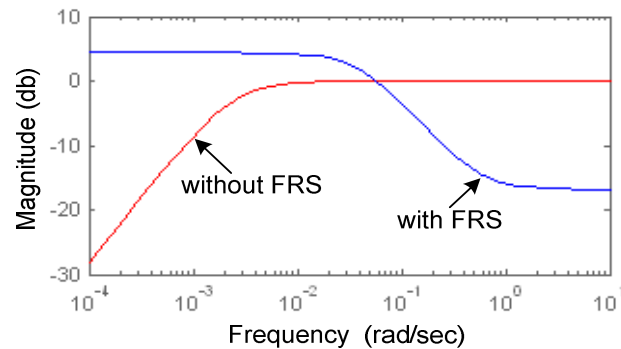


Figure 16. Yaw sensitive function with and without FRS

4.3. Interaction

Having independently discussed the rudder and fin control loop, the interactions between these two control loops should also be investigated. The degree of cross-coupling is established thus: the autopilot $K_{22}(s)$ response to yaw disturbance (yaw sensitivity function) with and without FYS control loop $K_{12}(s)$ is analyzed and then the FYS control loop $K_{11}(s)$ with and without the RRS control loop $K_{21}(s)$ is determined.

4.3.1. FYS Impact on Autopilot

The autopilot transfer function between the controlled yaw angle $\psi(s)$ and yaw disturbance $d_1(s)$ without FYS had been described in equation (14), and the autopilot transfer function with FYS is expressed as

$$\psi(s)/d_1(s) = 1/(1 + K_{22}(s)G_{22}(s) + K_{12}(s)G_{21}(s)) \quad (22)$$

Figure 17 depicts the sensitivity function obtained by employing the autopilot $K_{22}(s)$ with and without the FYS control loop $K_{12}(s)$. It is confidence that the ship yaw disturbance responses are mostly in the low frequency region (below 1.0 rad/sec), hence the autopilot $K_{22}(s)$ with and without FYS both could attenuate the yaw disturbance in the low frequency region. Furthermore, comparing to the controller without FYS, the controller with FYS has a larger tendency to attenuate the yaw disturbance, as can be noticed from the roll off feature at the low frequency region. This revealed that the frequency response of controller with FYS has little improvement in yaw disturbance attenuation performance.

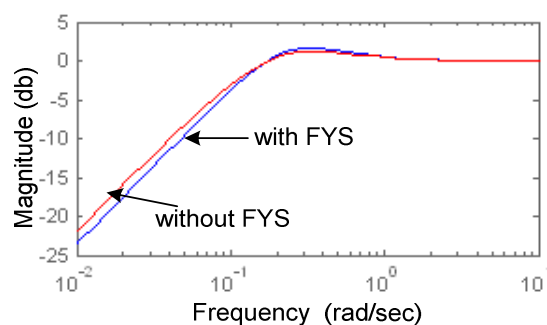


Figure 17. Yaw sensitive function with and without FYS

4.3.2. RRS Impact on FRS

The FRS transfer function without RRS between the controlled roll motion $\varphi(s)$ and roll disturbance $d_2(s)$ is described in equation (18), and the transfer function with RRS is expressed as

$$\varphi(s)/d_2(s) = 1/(1 + K_{11}(s)G_{11}(s)/K_{21}(s)G_{12}(s)) \quad (23)$$

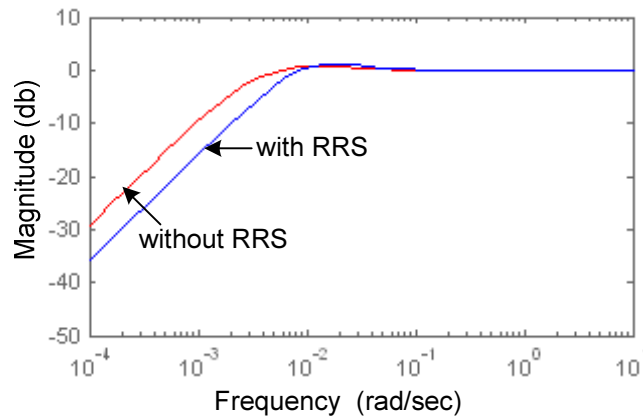


Figure 18. Roll motion response to disturbance with and without RRS

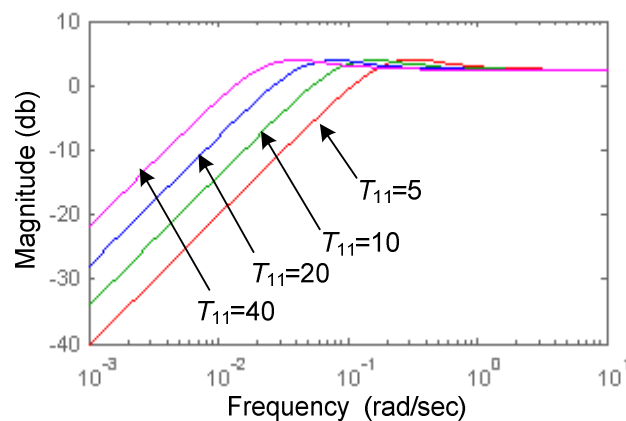


Figure 19. Changes in roll disturbance attenuation with different $T(s)$

Figure 18 depicts the roll disturbance characteristics by employing the FRS $K_{11}(s)$ with and without the RRS $K_{21}(s)$. It can be seen that the controller roll disturbance attenuation performance with the RRS was enhanced; this is often experienced in practice. Especially in lower frequency region, the degree of roll disturbance attenuation is improved considerably with the RRS, as can be noticed from the roll off feature of two cases. Also, we should notice that: because of the engineering constrains on the fin servomechanisms, such as slew rate, it is required that the higher frequency response of the controller must be restricted to prevent the fin saturation.

Furthermore, the degree of disturbances attenuation can easily be modified by varying the controller parameters of complementary sensitive function matrix $T(s)$. Taking the control channel FRS with the RRS as an example, as increasing the roll control loop bandwidth $1/T_{11}$, the desired roll disturbance attenuation performance could be achieved, as it is apparent in Figure 19. Therefore, the CGSA design method allows much greater flexibility in the controller design procedure by means of the effective selection of only two parameters of $T(s)$ which can be easily reflect through the system bandwidth.

5. Conclusion

In this paper, the CGSA technique is utilized to design the ship rudder and fin integrated controller. Through the frequency domain analysis of the various CGSA control loop and interactions between them, we can find that: the harmony use of the exiting rudder system and active fin roll stabilizer could provide a feasible method for roll reduction, whilst producing minimal yaw disturbance. Additionally, it must be noticed that: although the FYS with FRS has much better yaw disturbance attenuation performance, the FYS control loop could degrade the roll disturbance attenuation performance of FRS, which needs more consideration. Also this study has demonstrated the flexibility of the CGSA controller design procedure: throughout the suitable selection of the two controller parameters, the desired disturbance attenuation performance can be readily achieved. Hence, the integrated rudder and fin CGSA control scheme is very concise and indeed feasible for future practical application to ship integrated rudder and fin controller design.

References

- [1] Van Amerongen J, Van Klugt PGM, Van Der Pieffers JB. *Rudder roll Stabilization - Controller Design and Experimental Results*. Proceedings of 8th ship control system symposium. 1987; 1: 120-142.
- [2] Van Amerongen J, Van Klugt PGM, Van Nauta Lemke HR. *Rudder Roll Stabilization for Ships. Automatica*. 1990; 26(4): 679-690.
- [3] Roberts GN, Sharif MT, Sutton R, Agarwal, A. *Robust control methodology applied to the design a combined steering / stabilizer system for warships*. IEEE Proceedings of Control Theory Application. 1997; 144(2): 128-136.
- [4] Grimble MJ, Katebi MR, Zhang Y. *H_∞ Based Ship Fin/Rudder Roll Stabilisation Design*. 10th Ship Control System Symposium. 1993; 2: 245-265.
- [5] Sharif MT, Roberts GN, Sutton R. *Robust Fin/Rudder Ship Roll Stabilisation*. Proceedings of 3rd IEEE Conference on Control Applications. 1994; 2: 1107-1112.
- [6] Sharif MT, Roberts GN, Sutton, R. *Sea-trial Experimental Results of Fin/Rudder Roll Stabilisation. Control Engineering Practice*. 1995; 3(5): 703-708.
- [7] Yu P, Liu S. *Simulation on Nonlinear Rudder/Fin Joint Control Based on H_∞ Control Theory. Journal of System Simulation*. 2002; 14(8): 1040-1044.
- [8] Beaven RW, Wright MT, Seaward DR. *Weighting function selection in H_∞ design Process. Control Engineering Practice*. 1996; 4(5): 625-633.
- [9] Guan W, Su ZJ, Zhang GQ. *Concise Robust Control for MIMO System Based on Frequency Domain Analysis. Applied Mechanics and Materials*. 2013; (278-280): 1555-1560.
- [10] Guan W, Su ZJ, Zhang GQ. *CGSA Control Methodology Applied to Ship Integrated Rudder and Fin Stabilization System. Applied Mechanics and Materials*. 2013; (253-255): 2080-2085.
- [11] Blanke M, Christensen, AC. *Rudder-roll Damping Autopilot Robustness to Sway-Yaw-Roll Couplings*. 10th SCSS. Ottawa. 1993.
- [12] Yang LG, Zheng L. *Electromechanical device. Telkomnika*. 2012; 10(6): 1403-1408.
- [13] Hardiansyah, Junaidi. *Multiobjective H2/H Control Design with Regional Pole Constraints. Telkomnika*. 2012; 10(1): 103-112.
- [14] Grimble MJ, *Robust Industrial Control, Optimal Design Approach for Polynomial Systems*, Hempstead: Prentice-Hall. 1994.
- [15] Maciejowski JM, *Multivariable Feedback Design*. Wokingham: Addison-Wesley. 1989.
- [16] Roberts GN, Sharif MT, Sutton R, Agarwal A. *Robust control methodology applied to the design of a combined steering/stabilizer system for warships. Marine Control*. 1997; 3: 128-136.